Investigating the Crystalline Structure of Poly(vinylidene fluoride) (PVDF) in PVDF/Silica Binary and PVDF/Poly(methyl methacrylate)/ Silica Ternary Hybrid Composites Using FTIR and Solid-State ^{19}F MAS NMR Spectroscopy

Jin-Woo Park, Yun-Ah Seo, Il Kim, and Chang-Sik Ha*

Department of Polymer Science and Engineering, Pusan National University, Busan 609-735, Korea

Keitaro Aimi and Shinji Ando

Department of Organic and Polymeric Materials, Tokyo Institute of Technology, Ookayama 2-12-1, Meguro-Ku, Tokyo 152-8552, Japan

Received September 19, 2003; Revised Manuscript Received November 12, 2003

ABSTRACT: We investigated the crystalline structures of poly(vinylidene fluoride) (PVDF) in PVDF/silica (SiO_2) binary and PVDF/poly(methyl methacrylate) (PMMA)/SiO_2 ternary hybrid composite films using infrared (IR) analysis and solid-state, high-speed magic-angle-spinning (MAS) ^{19}F NMR spectroscopy. These hybrid films were prepared by sol−gel processes. We used three different blending sequences to prepare the ternary hybrid composite films: (1) The "Type 1" hybrid was prepared from a one-pot mixture of PVDF, PMMA, and tetraethoxysilane (TEOS), the silica precursor, in dimethylacetamide (DMAc). (2) The "Type 2" hybrid composite was prepared by first forming a PVDF/silica hybrid and then mixing it with PMMA. (3) The "Type 3" hybrid composite was prepared by mixing a preformed PMMA/silica hybrid with PVDF. The crystallinity of the PVDF/SiO_2 hybrid composite films decreased upon increasing the silica content. By using the different methods to prepare the PVDF/PMMA/SiO_2 ternary hybrid composite films, we were able to assign the γ-phase of PVDF crystals in the solid-state ^{19}F MAS NMR spectrum, which shows seven resonances that are attributable to an amorphous domain (−88 ppm), crystalline domains (−101.3, −93.7, −84.2, and −79.6 ppm), and regioirregular structures (−112.4 and −110.4 ppm). ^{19}F MAS NMR spectra of the Type 2 and Type 3 PVDF/PMMA/SiO_2 hybrid composite films show two new resonances, assignable to the γ-phase at lower (−101.3 ppm) and higher (−84.2 ppm) frequencies, which show long ^{19}F spin−lattice relaxation times in the rotating frame ($T_{1\rho}^{F}$) and chemical shifts that are significantly different from those of α- and β-phases of the PVDF crystals. The disappearance of the α-phase of PVDF crystals in the Type 2 and Type 3 hybrid composite films can be explained by the large silica particles in the PVDF/PMMA matrix hindering crystallization of PVDF. Solid-state ^{19}F spin-lock NMR spectroscopy experiments also indicate significant differences exist between the values of $T_{1\rho}^{F}$ of the crystalline and amorphous domains depending on the method of hybrid preparation.

Introduction

Poly(vinylidene fluoride) (PVDF) has remarkable electrical and mechanical properties. The discovery of its piezoelectrical[1] and pyroelectrical[2] properties has motivated most of its subsequent investigations. The poor optical clarity of PVDF, however, has limited its use as an optical material. In this regard, much emphasis has been placed on blending PVDF with an amorphous polymer, especially poly(methyl methacrylate) (PMMA), to improve its optical properties.[3]

PMMA and PVDF are molecularly miscible in the amorphous state and have been studied by thermal analysis,[4−6] dynamic mechanical spectroscopy,[5,7] X-ray scattering,[5,7] and Fourier transform IR (FTIR) spectroscopy.[8,9] Studies of PVDF/PMMA blends obtained either from the melt or from solution indicate that increasing the PMMA content results in an increase in the glass-transition temperature and a decrease in the melting and crystallization temperatures of PVDF.[6,10]

PVDF crystallizes in five different polymorphs, the so-called α, β, γ, δ, and ϵ forms.[11,12] The unit cell of the lattice of α-PVDF consists of two chains in *tg*+ *tg*− conformations. The dipole components are mutually antiparallel, and therefore, they neutralize each other; hence, α-PVDF exhibits nonpolar behavior. A polar analogue of α-PVDF is δ-PVDF, which is formed upon application of a high electric field.[13,14] PVDF polymorphs have been studied by a combination of differential scanning calorimetry (DSC), FTIR spectroscopy, and X-ray diffraction techniques.[15−17] Crystalline PVDF/PMMA blends consist of crystalline PVDF phases and miscible PVDF/PMMA amorphous phases. The morphology that PVDF/PMMA blends adopt depends on the cooling rate and the blend composition; together, these parameters determine whether PVDF crystallizes or remains amorphous upon cooling from the melt.

Solution-state ^{19}F NMR spectroscopy can provide insight into the chain microstructure of PVDF.[18] Recently, Holstein et al.[18] reported that after ^{1}H decoupling, PVDF powder obtained from the melt displays a major signal at $\delta_F = -91$ ppm, two shoulders at relatively lower and higher frequencies, and a weak doublet at a significantly lower frequency. The authors demonstrated that discrimination in favor of the crystalline domains is enhanced by a long spin-locking time. Solid-state spin-lock experiments show that significant differences exist in the ^{19}F spin−lattice relaxation times in the rotating frame ($T_{1\rho}^{F}$) between the immobile

* To whom correspondence should be addressed. E-mail: csha@pusan.ac.kr.

10.1021/ma035402g CCC: $27.50
Published on Web 12/17/2003

crystalline and mobile amorphous regions. The value of $T_{1\rho}^{F}$ is shorter for amorphous chains than it is for crystalline regions. In addition, the authors have shown, by partial conversion of the α form into the β form, that the β form displays a single signal at $\delta_F = -98$ ppm whereas the α-form displays two resonances at $\delta_F = -82$ and -98 ppm.[19,20]

One of us[20] has investigated the $^1H \rightarrow {}^{19}F/{}^{19}F \rightarrow {}^1H$ CP/MAS and inversion/recovery CP/MAS spectra of PVDF powder. The significant differences observed for the effective time constants, T^*_{HF} and $T^*_{1\rho}$, estimated from the $^1H \rightarrow {}^{19}F$ CP curves, clarify that significant differences exist in the strengths of the dipolar interactions between the crystalline and amorphous domains. In addition, the inverse $^{19}F \rightarrow {}^1H$ CP/MAS and $^1H \rightarrow {}^{19}F$ CP/drain MAS experiments provided information complementary to that from the $^1H \rightarrow {}^{19}F$ CP-MAS spectra.

Combining organic polymers with ceramics holds promise for the preparation of new high-performance hybrid materials.[21,22] Silica (SiO_2) is a material that has excellent mechanical, thermal, and optical properties. Yang and Bei[22] reported that, on the basis of their thermal stimulation discharge (TSD) studies, PVDF/silica composite films have good charge-storage ability and stability.

A simple method for obtaining an organic/inorganic hybrid is to mix an organic polymer with a metal alkoxide, such as tetraethoxysilane (TEOS), followed by a sol−gel process involving the hydrolysis and polycondensation of TEOS.[23] Fortunately, the sol−gel process provides new opportunities for preparing smart organic/inorganic hybrid materials at a relatively low temperature.

Although PVDF/PMMA blends have been investigated intensively, little is known about silica-containing hybrid composites based on PVDF or PVDF/PMMA blends. In this current study, therefore, we prepared PVDF/silica binary hybrid composites and PVDF/PMMA/silica ternary hybrid composite films by the sol−gel process. We conducted solid-state ^{19}F MAS NMR spectroscopic investigations to determine the crystalline structure of PVDF in these PVDF/SiO_2 binary and PVDF/PMMA/silica ternary hybrid composites. We used three different blending sequences to prepare the ternary hybrid composite films: (1) "Type 1" hybrids were formed from a one-pot mixture of PVDF, PMMA, and tetraethoxysilane (TEOS), as a precursor of silica, in dimethylacetamide (DMAc). (2) The "Type 2" hybrid composite was prepared by first forming a PVDF/silica hybrid and then mixing it with PMMA. (3) The "Type 3" hybrid composite was prepared by mixing a preformed PMMA/silica hybrid with PVDF. In this paper, we report the effects that silica has on the crystalline structure of PVDF in the hybrid composite films and how this phenomenon depends on the preparation method.

Experimental Section

Materials. The PVDF powder (M_n = 150 000; M_w = 300 000) that we used is KF-1100, which was supplied by Kureha Chemical Industry Co., Ltd. (Japan). The intrinsic viscosity of this PVDF is 1.1 dL/g in dimethylacetamide (DMAc) at 25 °C; it has about 3% structural defects (head-to-head or tail-to-tail bonds), as determined by ^{19}F NMR spectroscopy. PMMA (M_w = 120 000) was purchased from Aldrich. Tetraethoxysilane (TEOS) and hydrochloric acid (HCl) were purchased from Aldrich and Junsei, respectively, and used as received. DMAc was purchased from Aldrich and used without further purification.

Preparation of PVDF/Silica Binary Hybrid Composite Film. TEOS was used as a precursor to produce SiO_2. HCl and deionized water were introduced as the catalyst and hydrolysis reagent, respectively. First, a 10-wt % polymer solution was prepared by the dissolution of a requisite amount of PVDF powder in DMAc at room temperature. TEOS was then added dropwise slowly into the PVDF solution with vigorous stirring until a clear solution was obtained. It took ca. 1 h for TEOS to dissolve completely at room temperature. Once this clear solution was obtained, suitable amounts of HCl and deionized water were added to begin the sol−gel process. The SiO_2 content was either 5 or 10 wt %. The PVDF/SiO_2 sol solutions in DMAc were spin-coated onto a glass substrate at 500−1200 rpm for 30 s, and then the as-cast films were soft-baked at 150 °C for ca. 1 h. These soft-baked films were dried in a vacuum oven for 2 days at room temperature.

Preparation of PVDF/PMMA/Silica Ternary Hybrid Composite Films. We prepared three different types of ternary hybrid composite films, which we call Types 1−3. For the "Type 1" hybrid composite, the solid content of PVDF/PMMA mixture in the DMAc solution was 10 wt % and the weight ratio of PVDF/PMMA was 80/20. First, a 10-wt % polymer solution was prepared by the dissolution of a suitable amount of the PVDF/PMMA powders in DMAc at room temperature. TEOS was slowly added dropwise into the PVDF/PMMA solution with vigorous stirring until a clear solution was obtained. It took ca. 1 h for TEOS to dissolve completely at room temperature. Once the clear solutions were obtained, suitable amounts of HCl and deionized water were added to initiate the sol−gel reaction. The "Type 2" hybrid composite film was prepared by mixing PMMA with a PVDF/SiO_2 hybrid in DMAc. The "Type 3" hybrid composite film was prepared by mixing PVDF with a PMMA/SiO_2 hybrid in DMAc. This process was continued for 1 day in a jar roller mixer.

The SiO_2 content was fixed at 5 wt % for all of the different types of hybrid films. These films were dried under a dynamic vacuum oven for 4 days at room temperature.

Solid-State ^{19}F MAS NMR Measurements. Solid-state ^{19}F MAS NMR spectroscopic measurements were performed on a JEOL EX spectrometer. We operated the spectrometer at resonance frequencies of 282.65 and 300.40 MHz to obtain fluorine-19 and proton spectra, respectively. Samples were spun at the magic angle at rate of 16 kHz. Temperatures inside the rotor were calibrated using the ^1H chemical shifts of ethylene glycol absorbed in tetrakis(trimethylsilyl)silane spun at the same rate (16 kHz), and the ambient probe temperature was estimated to be 68 °C.[20] We used a commercial (Chemagnetics) $^1H-{}^{19}F$ double-tuned APEX MAS probe capable of high-power heteronuclear decoupling and fitted with a 4-mm o.d. zirconia Pencil. The ^{19}F spin−lattice relaxation times in the rotating frame ($T_{1\rho}^{F}$) were measured at a spinning speed of 16 kHz using the H−F probe by means of the variable-time spin-lock technique. Chemical shifts in ^{19}F NMR spectra are quoted with respect to the signal for $CFCl_3$ and were measured via replacement with a sample of liquid C_6F_6 (−163.6 ppm) with proton decoupling. The recycle delays of 5.0 s were sufficiently long compared with the spin−lattice relaxation time in the laboratory frame of the sample (T_1^F = 0.5 s; T_1^H = 0.8 s). In this study, the magnitude of the ^1H decoupling was ca. 75 kHz.

Solution ^{19}F NMR Measurements. Solution ^{19}F NMR measurements were performed on a JEOL GSX-500 spectrometer at a resonance frequency of 470.4 MHz for ^{19}F nuclei at 60 °C. Samples were dissolved in dimethyl sulfoxide-d_6 at the concentration of 1.5 wt %. The spectra were acquired using single-pulse excitation with a 30° pulse duration, recycle delay of 5 s, spectral width of 100 kHz, and 400 transients. ^{19}F chemical shifts are quoted with respect to the signal for $CFCl_3$ dissolved in the solvent.

Results

PVDF/SiO_2 Binary Hybrid Composite Films. In this study, we identified the crystalline phases of PVDF

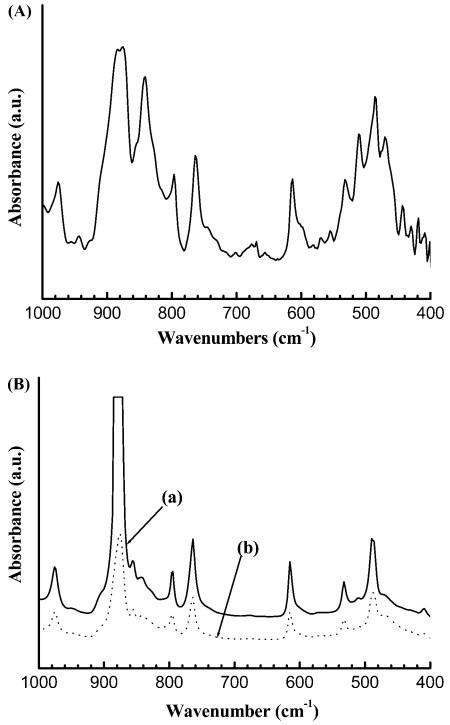

Figure 1. FTIR spectra of (A) PVDF and (B) PVDF/SiO_2 hybrid composite films with two different SiO_2 contents: (a) 5 wt % and (b) 10 wt %.

by using FTIR spectroscopy and solid-state ^{19}F MAS NMR spectroscopy. Figure 1 displays the IR spectra of PVDF/SiO_2 binary composite films having two different SiO_2 contents as well as that of a sample of PVDF homopolymer. Gregorio and Cestari[17] reported IR absorption bands that are characteristic to the α-phase (531, 612, 766, 795, 855, and 976 cm^{-1}), β phase (470, 511, and 840 cm^{-1}), and γ-phase (835, 815, 776, 510, and 430 cm^{-1}).[15,16,24] Figure 1 displays the IR spectra of the PVDF powder and the PVDF/SiO_2 binary hybrid composite films that were annealed at 150 °C for 1 h. We observe many of the features associated with the α-phase but no characteristic features of the β- and γ-phases. These IR spectroscopy results suggest that the PVDF powder and PVDF/SiO_2 hybrids are composed of α-phases, regardless of the SiO_2 content.

Figure 2 displays the solid-state ^{19}F MAS NMR spectra of solid PVDF powder[19,20,25] and PVDF/SiO_2 binary hybrid composite films. These spectra, which can be fitted by a combination of five Lorentzian functions,[20] exhibit five isotropic resonances, as reported by Harris and co-workers, that we attribute to amorphous domains (−88.5 ppm), a crystalline domain (−93.7 and −79.6 ppm), and regioirregular structures (−112.4 and −110.4 ppm).[19,20,26] Ferguson and Brame[27] suggested, on the basis of solution-state NMR spectra, that the CF_2 fluorine atoms in head-to-head (CF_2–CH_2–CF^*_2–CH_2–CH_2–) sequences, which are located in the amorphous domain, resonate at lower frequency, by 3.2 ppm, than do those of the head-to-tail sequence (the major signal); this situation was confirmed recently by Scheler[28] and Wormald et al.[14] with the aid of $T_{1\rho}^F$-filtered radio frequency-driven recoupling (RFDR) and spin-diffusion experiments.

The values of $T_{1\rho}^F$ of each peak in the spectra in Figure 2 can be estimated from the decays of ^{19}F magnetization by conducting variable ^{19}F spin-lock time (t_{SL}) experiments. Table 1 summarizes the directly

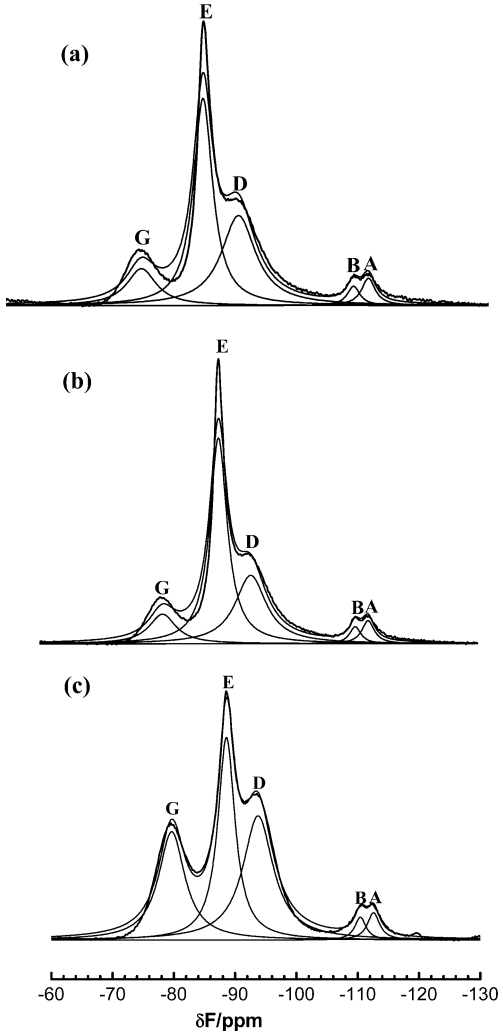

Figure 2. ^{19}F MAS NMR spectra of (a) PVDF/SiO_2 (5 wt %), (b) PVDF/SiO_2 (10 wt %), and (c) PVDF powder. The spectra were decomposed using five Lorentzian functions.

measured values of $T_{1\rho}^F$ that we obtained by fitting the decays using single- or double-exponential functions. The decays of the crystalline peaks have very long $T_{1\rho}^F$ components. This phenomenon agrees well with the fact that the magnetization of the crystalline domain is retained after a long spin-lock time (20 ms), as shown in Figure 3. These crystalline-selective spectra clearly indicate that the PVDF powder and the PVDF/silica binary hybrid composite films have characteristics of the α-phase,[18] which is in good agreement with the IR spectroscopy results. We assign the shoulder peak that resonates at −88 ppm to the residual amorphous signals that were not completely relaxed even after a spin-lock time of 20 ms.

The IR spectra displayed in Figure 1 indicate that the incorporation of SiO_2 nanoparticles does not affect the crystalline structure of PVDF. Likewise, in Figure 2, there is not much difference between the NMR spectra of the PVDF/SiO_2 binary hybrid composite films, except for the significant decrease in the relative intensities of the crystalline peaks (D and G) upon increasing the SiO_2 content. It is not surprising, however, that the crystallinity of PVDF decreases when increasing the SiO_2 content, because dispersed SiO_2 particles in the hybrid composite may interfere with PVDF crystal growth. From Table 2 we see that the crystallinity of PVDF in the PVDF/silica binary hybrid composite films,

Table 1. Spin−Lattice Relaxation in the Rotating Frames of Each Spectral Component in the Solid-State ^{19}F MAS NMR Spectra of PVDF Powder and PVDF/SiO_2 Hybrid Composite Films

sample	chemical shift (ppm) width at half-heightsymbol	−112.41.2A	−110.41.1B	−93.73D	−88.51.7E	−79.62.6G
PVDF powder	relative intensity (%)[b]	3	2	35	33	27
	$T_{1\rho}^F$ (ms)	1.2 (32%)	2.9 (26%)	0.4 (25%)	1.5 (17%)	0.3 (10%)
		11.3 (68%)	14.6 (74%)	35.1 (75%)	8.0 (83%)	49.6 (90%)
PVDF/SiO_2 (5 wt %)[a]	relative intensity (%)[b]	4	3	35	46	12
	$T_{1\rho}^F$ (ms)	1.1 (45%)	2.2 (47%)		2.6 (62.8%)	
		8.1 (55%)	9.4 (53%)	20.2 (100%)	8.0 (37.2%)	36.8 (100%)
PVDF/SiO_2(10 wt %)[a]	relative intensity (%)[b]	4	3	29	52	12
	$T_{1\rho}^F$ (ms)	0.8 (34%)	2.2 (47%)		2.5 (69%)	
		11.4 (64%)	9.4 (53%)	15.6 (100%)	7.6 (31%)	32.6 (100%)

[a] Hybrid composite film. [b] Error ±0.5%

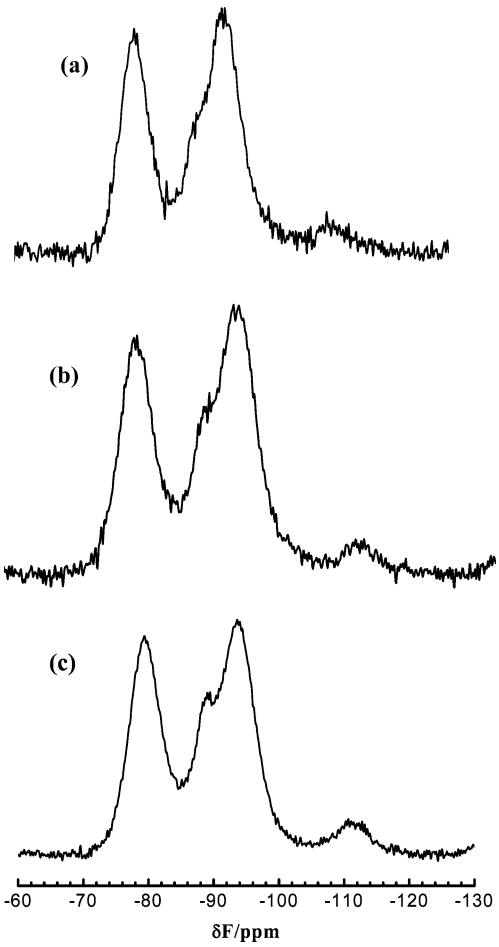

Figure 3. Crystalline-selective NMR spectra of (a) PVDF/SiO_2 hybrid composite film (5 wt %), (b) PVDF/SiO_2 hybrid composite film (10 wt %), and (c) PVDF powder. Conditions: spin-locked for 20 ms, 16 kHz.

Table 2. Proportions of the Amorphous, Crystalline, and Regioirregular (head-to-head and tail-to-tail) Components Determined from Solid-State ^{19}F MAS NMR Spectroscopy (error ±0.5 %)

	PVDF powder	PVDF/SiO_2 (5 wt %)	PVDF/SiO_2 (10 wt %)
amorphous regions (%)	33	46	52
crystalline regions (%)	61	47	41
regioirregular part (%)	6	7	7

which we estimated by deconvolution of the directly polarized ^{19}F NMR spectra, decreased from 61.9% (PVDF powder) to 41.6% (10 wt % SiO_2) upon increasing the silica content. This result is in good agreement with our previous DSC results,[23] in which the degree of crystallinity of PVDF was found to decrease from 59.6%

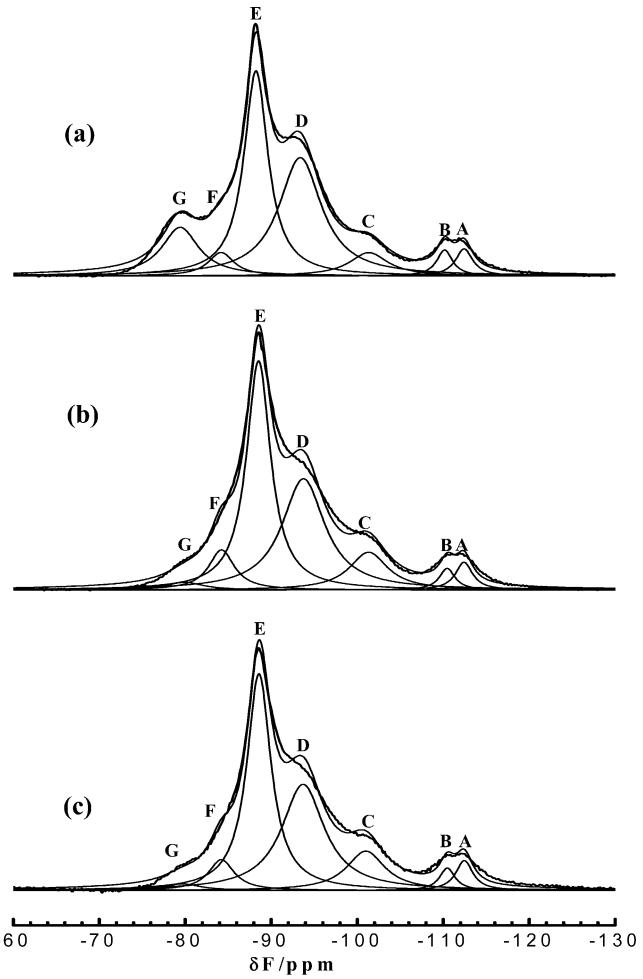

Figure 4. ^{19}F MAS NMR spectra of PVDF/PMMA/SiO_2 of (a) Type 1, (b) Type 2, and (c) Type 3. The spectra were decomposed using seven Lorentzian functions.

to 49.3% when increasing the content of SiO_2 from 0 to 10 wt %. Therefore, we conclude from both the IR and NMR spectroscopic analyses that the crystalline structure of PVDF is not changed very much upon addition of SiO_2.

PVDF/PMMA/SiO_2 Ternary Hybrid Composite Films. We investigated the crystalline structure of PVDF in the PVDF/PMMA/SiO_2 ternary hybrid composite film with the aid of IR and ^{19}F MAS NMR spectroscopy. Figure 4 displays the ^{19}F MAS NMR spectra of these films. We note that all of the PVDF/PMMA/SiO_2 ternary hybrid composite films display distinct shoulders at low (−101.3 ppm; C) and high (−84.2 ppm; F) frequencies along with five isotropic resonances (−112.4, −110.4, −93.7, −88.5, and −79.6

Table 3. Spin−Lattice Relaxation in the Rotating Frames of Each Spectral Component in the Solid-State ^{19}F MAS NMR Spectra of the γ-Form PVDF Film and PVDF/PMMA/SiO_2 Hybrid Composite Films

sample	chemical shift (ppm) width at half-height symbol	−112.4 1.2 A	−110.4 1.1 B	−101.3 2.7 C	−93.7 3 D	−88.5 1.7 E	−84.2 1.8 F	−79.6 2.6 G
PVDF/PMMA/SiO_2 (Type 1)[a]	relative intensity (%)[b]	3	3	6	36	35	4	13
	$T_{1\rho}^F$(ms)	1.1 (60%)	2.1 (66%)	1.1 (47%)	0.6 (39%)	1.2 (40%)		
		10.2 (40%)	10.1 (34%)	34.6 (53%)	17.4 (61%)	4.3 (60%)	12.2 (100%)	23.5 (100%)
PVDF/PMMA/SiO_2 (Type 2)[a]	relative intensity (%)[b]	4	3	12	34	38	6	3
	$T_{1\rho}^F$(ms)	1.4 (57%)	2.2 (56%)		0.9 (32%)	1.4 (42%)	2.8 (46%)	
		8.7 (43%)	8.7 (44%)	24.0 (100%)	11.5 (68%)	5.1 (58%)	14.8 (54%)	21.3 (100%)
PVDF/PMMA/SiO_2 (Type 3)[a]	relative intensity (%)[b]	3	2	11	34	41	7	2
	$T_{1\rho}^F$(ms)	1.7 (37%)	1.6 (41%)	0.3 (25%)	0.9 (30%)	1.1 (30%)	4.7 (38%)	
		5.9 (63%)	6.8 (59%)	48.6 (75%)	11.5 (70%)	4.6 (70%)	34.5 (62%)	25.6 (100%)
γ-form PVDF film	relative intensity (%)[b]	4	3	8	28	48	4	5
	$T_{1\rho}^F$(ms)	1.5 (67%)	1.7 (51%)	6.1 (22%)	1.6 (24%)	1.8 (59%)		
		12.2 (33%)	8.5 (49%)	22.2 (78%)	18.7 (76%)	6.8 (41%)	17.1 (100%)	22.1 (100%)

[a] Hybrid composite film. [b] Error ±0.5%.

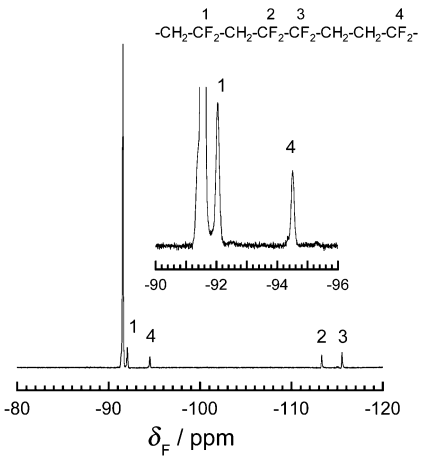

Figure 5. Solution-state ^{19}F NMR spectrum of PVDF dissolved in dimethyl sulfoxide-d_6.

ppm). The origin of these new signals (C and F) is discussed below. Figure 5 shows the solution-state ^{19}F NMR spectrum of PVDF dissolved in dimethyl sulfoxide-d_6. The signal assignments of the four small peaks (1−4) attributable to the regioirregular sequences are also included in the figure.[29] Peaks 2 and 3 resonated at −113.2 and −115.5 ppm are clearly observed in the solid-state NMR spectra as peaks B and A, whereas the other peaks 1 and 4 resonated at −92.0 and −94.5 ppm should be overlapped with peaks E and D, respectively. In contrast, no signals are observed around −84.0 and −98.0 ppm in the solution spectrum, at which the distinct peaks of F and C are observed in the solid-state MAS spectrum. This clearly indicates that these peaks should be originated from the polymorphs of crystalline domains. Table 3 summarizes the values of $T_{1\rho}^F$. The long values of $T_{1\rho}^F$ observed for the shoulders C and F indicate that these signals can be assigned in a straightforward manner to the immobile crystalline phase. In addition, these shoulders are observed clearly in the crystalline-selective spectra (Figure 6). These facts indicate that the ^{19}F NMR spectra of these films are not consistent with the previously reported typical crystalline-selective spectra of PVDF. The four peaks observed for the crystalline regions of the PVDF/PMMA/SiO_2 ternary hybrid composite films cannot be assigned to either the α or β phase. It is also noteworthy from the data in Table 3 that the ratios of the intensities of peaks C and F relative to the sum of the total peak intensities for the Type 2 and Type 3 hybrid composite films are higher than those for the Type 1 hybrid composite film.

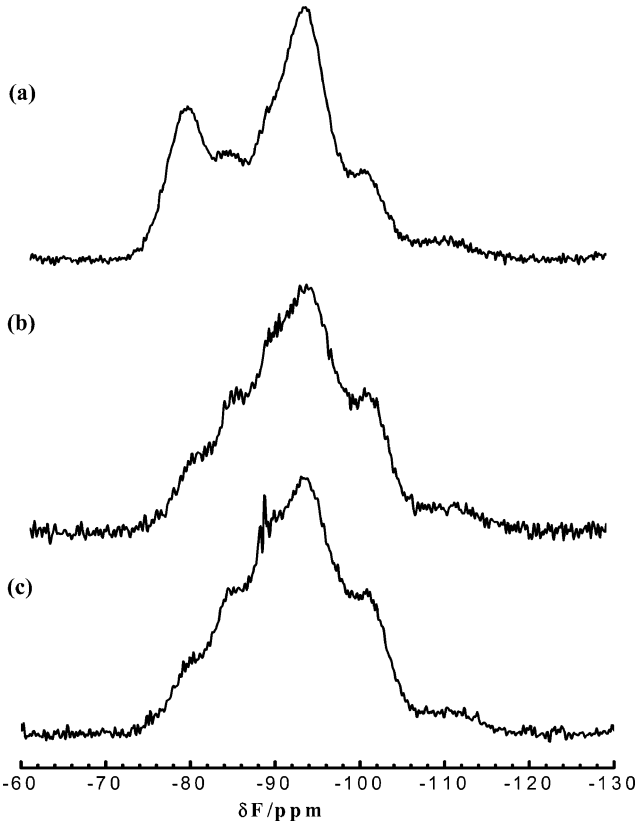

Figure 6. Crystalline-selective NMR spectra of PVDF/PMMA/SiO_2 hybrid composite films of (a) Type 1, (b) Type 2, and (c) Type 3. Conditions: spin-locked for 20 ms, 16 kHz.

Discussion

Figure 7 displays the IR spectra of the PVDF/PMMA/SiO_2 ternary hybrids that we recorded to obtain more detailed information about the nature of the crystalline phase of PVDF in the PVDF/PMMA/SiO_2 ternary hybrids. Although the peaks at 976, 855, 795, and 766 cm^{-1} are all assignable to the α phase, we believe that the bands at 835 and 815 cm^{-1} characterize the γ-phase; these peaks are indicated by arrows. The results of this IR spectral analysis, therefore, indicate that the Type 1 film is composed of α and γ phases. It is noteworthy, however, that the Type 2 and Type 3 films are almost entirely composed of the γ phase. Therefore, we suggest that peaks C and F in the ^{19}F MAS spectra can be assigned to the γ phase.

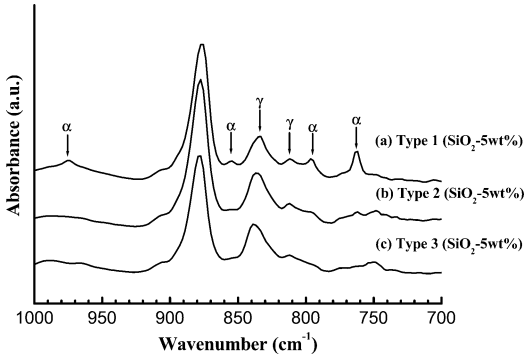

Figure 7. FTIR spectra of PVDF/PMMA/SiO_2 hybrid composite films. Although the peaks at 976, 855, 795, and 766 cm^{-1} are all assignable to the α phase, the bands at 835 and 815 cm^{-1} are believed to be assignable to the γ phase; those peaks are indicated by arrows.

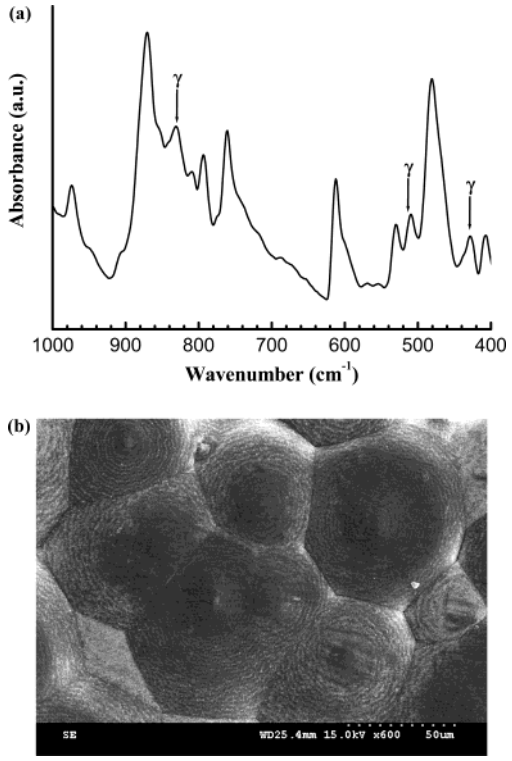

Figure 8. (a) FTIR spectrum (the bands at 835, 510, and 430 cm^{-1} are all assignable to the γ phase; those peaks are indicated by arrows) and (b) scanning electron microscope image of the γ-form of the PVDF film. Conditions: annealed for 12 h at 170 °C.

To prove this point, we prepared typical PVDF films of the γ-phase. These films were prepared by annealing spin-coated PVDF films at 170 °C for 12 h, followed by cooling at a normal rate (e.g., 10−20 °C/min or higher).[30] Figure 8a displays the IR spectra of annealed PVDF films. The bands at 835, 510, and 430 cm^{-1}, which are indicated by arrows, are all assignable to the γ-phase. Moreover, a scanning electron microscopy image (Figure 8b) of the annealed PVDF films clearly exhibits a spherulitic γ phase.[11,23a] We attempted to characterize this γ-form film by solid-state NMR spectroscopy. Figure 9a displays the ^{19}F MAS NMR spectrum, which exhibits two new peaks at −84.2 and −101.3 ppm in addition to five peaks at −79.6, −88.5, −93.7, −110.4, and −112.4 ppm. Table 3 summarizes the directly measured values of $T_{1\rho}^F$ that we obtained using single- or double-exponential functions. The decays of the crystalline

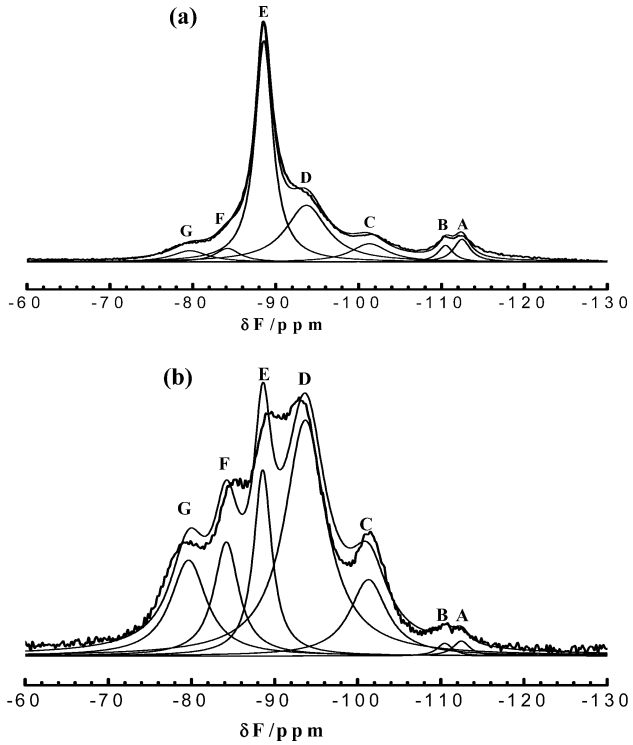

Figure 9. Comparison of (a) directly polarized and (b) crystalline-selective ^{19}F NMR spectra of γ-form PVDF film. The spectra were decomposed using seven Lorentzian functions. Conditions: spin-locked time for 20 ms (b), 16 kHz.

peaks (D and G) and new peaks (C and F) have long $T_{1\rho}^F$ components; the amorphous peaks (A, B, and E) have relatively short $T_{1\rho}^F$ components. The results of these measurements of decay in ^{19}F spin-lock experiments, therefore, indicate that the new peaks are assignable to the crystalline phase. In the $T_{1\rho}^F$ measurement and the ^{19}F MAS NMR spectra, the PVDF film having the γ-crystalline form exhibits seven resonances that we attribute to amorphous domains (−88.5 ppm), crystalline domains (−101.3, −93.7, −84.2, and −79.6 ppm), and regioirregular structures (−112.4 and −110.4 ppm). It should be noted that peak D, which is attributed to the crystalline phase, exhibits significant proportions of short $T_{1\rho}^F$ components (0.6−1.6 ms). As described above, peaks E and D contain the contributions from the regioirregular sequences demonstrate as peak 1 and 4 in the solution spectra (Figure 5). Hence, the short $T_{1\rho}^F$ components observed for peak D should not be ascribed to the rigid crystalline domain but to the regioirregular sequences located in the mobile amorphous domain.

The crystalline-selective spectra of PVDF film having the γ-crystalline form are presented in Figure 9b. Careful inspection of Figures 4 and 9 indicates that the relative intensity of peak G (−79.6 ppm) in the PVDF/PMMA/SiO_2 ternary hybrid film (Type 1) is larger than that observed for the γ-form PVDF film (Types 2 and 3). From the IR spectroscopy data (Figure 7), the Type 1 film is composed of α and γ phases but Types 2 and 3 consist almost entirely of the γ phase. This observation indicates that peak G can be assigned to the α-crystalline form. Since the crystalline α-form PVDF exhibits two peaks having the same signal intensities,[19] the other α-crystalline signal should be observed at peak D. Although β-form PVDF exhibits a single signal for the crystalline region at the same position as peak D, the IR spectra provide no evidence for the β-crystalline form

for Type 2 and Type 3 hybrids. Therefore, we suggest that the C, D, and F peaks can be assigned to the γ form, although peak D is overlapped with the lower frequency peak of the α form. On the other hand, peak E in Figure 9b is assignable to the signal of the residual amorphous form.

We now discuss how the differences in the crystalline structure of PVDF in the binary and ternary hybrid composite films depend on the preparation sequence. We observed only the α phase for PVDF crystals in all the binary and ternary hybrid composite films, as well as the PVDF film, regardless of the preparation sequence, when they were prepared at room temperature and then annealed at 150 °C for ca. 1 h. It is interesting that we observe mainly the γ phase for both the Type 2 and Type 3 ternary hybrid composite films and both α and γ phases for the Type 1 ternary hybrid composite films, as well as the PVDF/silica binary hybrid composite film and the PVDF film, when they were prepared at room temperature without annealing. These results strongly suggest that silica has a different effect on the crystalline structure of PVDF depending on the status of the silica before and after the sol−gel reaction.

For the Type 1 ternary hybrid composite film, PVDF is crystallized in the presence of both PMMA molecular chains and TEOS, since the sol−gel reaction takes place simultaneously with the solvent drying process at room temperature. In this case, the size of the silica particles prepared during the sol−gel process is not that large, and thus, these silica particles do not significantly affect the crystallization of PVDF. The same effect occurs for the PVDF/silica binary hybrid composite film. For the Type 2 and 3 hybrid films, however, PVDF is crystallized in the presence of the slightly larger silica particles in PMMA or PVDF matrix, since these films were prepared from a mixture of PMMA or PVDF and preformed PVDF/silica (Type 2) or PMMA/silica (Type 3) hybrid films. In these cases, we expect that the particle sizes of the silica are much larger than those found in the Type 1 film because the silica particles present in the PVDF or PMMA matrix have already formed networks during the completed sol−gel process. Therefore, the ^{19}F MAS NMR (Figures 4, 6, and 9) and FTIR (Figure 8) spectra strongly suggest that the presence of the relatively large silica particles significantly hinders the formation of the most favorable α-phase PVDF crystals and, thus, reduces the relative ratio of α phase with respect to the total mixed α and γ phases, which results in the clear formation of γ phase PVDF crystals for both Type 2 and Type 3 hybrid films.

The interactions between PVDF and PMMA, if there are any, do not seem to affect the crystalline structure of PVDF in the ternary hybrid composite films because there is no difference between the results for the Type 2 and Type 3 hybrid composite films, regardless of the blending sequence, whether the silica particles are located in the amorphous part of PVDF or in the PMMA matrix.

Conclusions

We prepared PVDF/silica binary hybrid composite films and PVDF/PMMA/silica ternary composite films by the sol−gel method. Three different blending sequences were utilized to prepare the ternary hybrid composite films: (1) mixing a one-pot mixture of PVDF, PMMA, and TEOS in DMAc (Type 1); (2) mixing a preformed PVDF/silica hybrid with PMMA (Type 2); (3) mixing a preformed PMMA/silica hybrid with PVDF (Type 3). We investigated the crystalline structures of the PVDF/SiO_2 and PVDF/PMMA/SiO_2 hybrid composite films by FT-IR and solid-state ^{19}F MAS NMR spectroscopy. ^{19}F MAS NMR spectra obtained from spin-lock experiments are very sensitive to the crystalline structures of PVDF, and hence, the relative population and molecular mobility of each morphological component could be estimated quantitatively. ^{19}F MAS NMR spectra of PVDF/PMMA/SiO_2 hybrid composite films (Types 2 and 3) display two new distinct shoulders at lower (−101.3 ppm) and higher (−84.2 ppm) frequencies; they possess long values of $T_{1\rho}^{F}$ (typical for crystalline components), and their chemical shifts are significantly different from those of the α and β phases. The ^{19}F MAS NMR spectrum of γ-form PVDF, which was prepared by annealing at 170 °C for 12 h, exhibits four crystalline peaks at the same chemical shifts of the hybrids of Types 2 and 3. Thus, we were able to successfully assign the γ form of PVDF crystals by preparing PVDF/PMMA/SiO_2 ternary hybrid composite films by different preparation sequences.

Acknowledgment. This work was supported partly by the KAIST-TIT Joint Exchange Program through the KOSEF and JSPS sponsorship and partly by a Grant-in-Aid for scientific research (No.13450387) from the JSPS. C.S.H. thanks the National Research Laboratory Program, the Center for Integrated Molecular Systems, POSTECH, Korea, and the Brain Korea 21 Project for their financial support. S.A. is grateful to Prof. Harris for helpful discussions.

References and Notes

(1) Geschke, D.; Leister, N.; Steffen, M.; Glasel, H. J.; Hartmann, E. *J. Mater. Sci. Lett.* **1997**, *16*, 1943.
(2) Bergman, J. G.; McFee, J. H.; Crane, G. R. *Appl. Phys. Lett.* **1971**, *18*, 203.
(3) Roerdrink, E.; Challa, G. *Polymer* **1978**, *19*, 73.
(4) Noland, J. S.; Hsu, N. N.-C.; Saxon, R.; Schmitt, J. M. *Adv. Chem. Ser.* **1971**, *99*, 15.
(5) Paul, D. R.; Altamirano, J. O. *Adv. Chem. Ser.* **1975**, *142*, 371.
(6) Nishi, T.; Wang, T. T. *Macromolecules* **1975**, *8*, 909.
(7) Hirata, Y.; Kotaka, T. *Polym. J.* **1981**, *13*, 273.
(8) Coleman, M. M.; Zarrian, J.; Varnel, D. F.; Painter, P. C. *J. Polym. Sci. Lett. Ed.* **1977**, *15*, 745.
(9) Bernstein, R. E.; Cruz, C. A.; Paul, D. R.; Barlow, J. W. *Macromolecules* **1977**, *10*, 681.
(10) Rinaldo, G., Jr.; Nadia, C. P. J. *Phys. D: Appl. Phys.* **1995**, *28*, 432.
(11) Lee, W. K.; Ha, C. S. *Polymer* **1998**, *39*, 7131.
(12) Lu, F. J.; Hsu, S. L. *Macromolecules* **1986**, *19*, 326.
(13) Lovinger, A. J. *Science* **1983**, *220*, 1115.
(14) Wormald, P.; Apperley, D. C.; Harris, R. K. *Polymer* **2003**, *44*, 643.
(15) Lovinger, A. J., *Macromolecules* **1981**, *14*, 322.
(16) Bachmann, M. A.; Gordon, W. L.; Koenig, J. L.; Lando, J. B. *J. Appl. Phys.* **1979**, *50*, 6160.
(17) Gregorio, G., Jr.; Cestari, M. *J. Polym. Sci., Part B*: *Polym. Phys.* **1994**, *32*, 859.
(18) Holstein, P.; Harris, R. K.; Say, B. J. *Solid State Nucl. Magn. Reson.* **1997**, *8*,
(19)
(20) Robin, K.; Harris, R. K.; Holstein, P. *Polymer* **1998**, *39*, 4937.
(21) Ando, S.; Harris, R. K.; Reinsberg, S. A. *Magn. Reson. Chem.* **2002**, *40*, 97.
(22) Tajitsu, Y.; Yonezawa, M.; Sato, A.; Tomiyama, H.; Date, M.; Fukada, E. *Jpn.*
(23) *J. Appl. Phys.* **2000**, *39*, 5672.
(24) Yang, D.; Bei, W. *Proceeding of the IEEE International Symposium on Electrical Insulation*, Montreal, Quebec, June 5−8, **1994**, p 590.

(25) (a) Kim, J. W.; Cho, W. J.; Ha, C. S. *J. Polym. Sci., Part B: Polym. Phys.* **2002**, *40*, 19. (b) Ha, C. S.; Park, H. D.; Frank, C. W. *Chem. Mater.* **2000**, *12*, 839. (c) Park, H. D.; Ahn, K. Y.; Wahab, M. A.; Kim, I.; Jo, N. J.; Ha, C. S.; Lee, W. K.; Kim, G. H. *Macromol. Res.* **2003**, *11* (3), 172. (d) Guo, W.; Park, J. Y.; Oh, M. O.; Jeong, H. W.; Cho, W. J.; Kim, I.; Ha, C. S. *Chem. Mater.* **2003**, *15*, 2295.

(26) Tashiro, K.; Kobayashi, K.; Tadokoro, H. *Macromolecules* **1981**, *14*, 1757.

(27) Su, T. W.; Tzou, D. L. *Polymer* **2000**, *41*, 7289.

(28) Ando S.; Harris, R. K.; Scheler, U. *Advances in NMR; Fluorine-19 NMR of Solids Containing Both Fluorine and Hydrogen; Supplement of the Encyclopedia of Nuclear Magnetic Resonance*; John Wiley & Sons: Chichester, U.K., 2002; Vol. 9, pp 531−550.

(29) Ferguson, R. C.; Brame, E. G. *J. Phys. Chem.* **1979**, *83*, 1397.

(30) Scheler, U. *Bull. Magn. Reson.* **1999**, *19*, 52.

(31) Tonelli, A. E.; Schilling, F. C.; Cais, R. E. *Macromolecues* **1982**, *15*, 849.

(32) Hasegawa, R. *Polym. J.* **1972**, *3*, 591.

MA035402G